Transverse-Field Ising Dynamics in a Rydberg-Dressed Atomic Gas

V. Borish, O. Marković, J. A. Hines, S. V. Rajagopal, and M. Schleier-Smith

Phys. Rev. Lett. **124**, 063601 — Published 11 February 2020

DOI: 10.1103/PhysRevLett.124.063601

Transverse-Field Ising Dynamics in a Rydberg-Dressed Atomic Gas

V. Borish,[1] O. Marković,[2] J. A. Hines,[1] S. V. Rajagopal,[2] and M. Schleier-Smith[2]

[1]*Department of Applied Physics, Stanford University, Stanford, California 94305, USA*
[2]*Department of Physics, Stanford University, Stanford, California 94305, USA*

(Dated: January 9, 2020)

We report on the realization of long-range Ising interactions in a cold gas of cesium atoms by Rydberg dressing. The interactions are enhanced by coupling to Rydberg states in the vicinity of a Förster resonance. We characterize the interactions by measuring the mean-field shift of the clock transition via Ramsey spectroscopy, observing one-axis twisting dynamics. We furthermore emulate a transverse-field Ising model by periodic application of a microwave field and detect dynamical signatures of the paramagnetic-ferromagnetic phase transition. Our results highlight the power of optical addressing for achieving local and dynamical control of interactions, enabling prospects ranging from investigating Floquet quantum criticality to producing tunable-range spin squeezing.

Optically controlled interactions among cold atoms are a powerful tool for fundamental studies of quantum many-body dynamics [1–19] and for engineering entangled states [20–27]. Tailoring interactions with light theoretically allows for accessing non-equilibrium phases of matter [16, 28–30], studying inhomogeneous quantum phase transitions [31], implementing quantum optimization algorithms [32, 33], and enhancing quantum sensors [34–36]. Demonstrated approaches to optical control include coupling atoms to Rydberg states [1–9, 20–24], optical resonators [10–12, 25, 26], or molecular bound states [13, 14, 37–41]. Among these approaches, Rydberg excitation is notable for producing strong interactions on the few-micron scale—a typical interatomic spacing in a laser-cooled gas or optical tweezer array [4–6].

An alternative to direct excitation is Rydberg dressing, i.e., inducing interactions among ground-state atoms by coupling to Rydberg states with an off-resonant laser field [17–19, 27]. Rydberg dressing offers the benefit of dynamical control over the strength and form of interactions, as well as a long coherence time once the light is switched off. Maximizing the coherence of the interactions themselves has been the focus of several recent experiments [42–45]. While dressing in dense 3D lattices has suffered from runaway loss and dephasing [44–46], Rydberg dressing has been successfully applied for electrometry in a bulk gas [47], entangling atoms in optical tweezers [24], and studying coherent many-body spin dynamics in one- and two-dimensional atom arrays [2, 3].

The simplest form of interaction realizable by Rydberg dressing is an Ising interaction, where the Ising spins are encoded in two hyperfine ground states. Applications in quantum simulation [16], quantum optimization [32, 33], and quantum state engineering [36] additionally require a transverse field, which allows quantum correlations to spread. The transverse-field Ising model can undergo a phase transition from paramagnetic to ferromagnetic, which has been studied in mean-field dynamics of Bose-Einstein condensates [48] and in trapped-ion spin chains [49, 50]. The dynamics of spin correlations in this model have been investigated by direct Rydberg excitation [8, 9]. Time-dependent variants of the model furthermore yield a rich diagram of Floquet phases, including time crystals [28, 51] and predicted Floquet symmetry-protected topological phases [16, 28, 29].

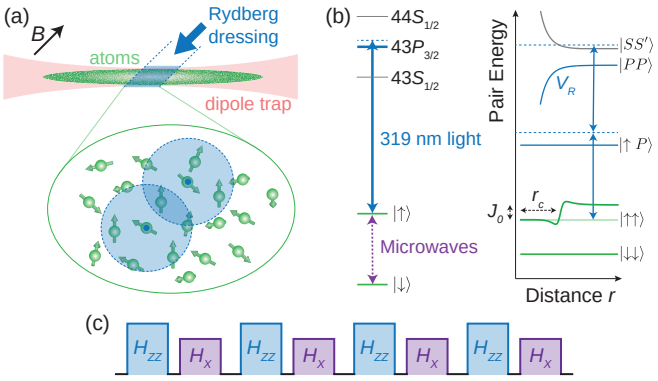

FIG. 1. **Experimental setup and Rydberg dressing scheme.** (a) A cloud of cesium atoms is held in an optical dipole trap and locally illuminated with 319 nm light to generate Ising interactions of characteristic range r_c and strength J_0. The quantization axis is set by a 1 G magnetic field $\mathbf{B}$. (b) Energy level diagrams for a single atom (left) and for a pair of atoms (right). (c) Alternating between interactions (H_{ZZ}) and microwave rotations (H_X) produces an effective transverse-field Ising model.

In this Letter, we report on the realization of a transverse-field Ising model in a dilute gas of Rydberg-dressed cesium atoms. For spins encoded in the hyperfine clock states, we generate interactions extending over a range of several microns by coupling to Rydberg states near a Förster resonance. At the mean-field level, the Ising interactions manifest as one-axis twisting dynamics [52, 53], which we observe by Ramsey spectroscopy [2, 54]. We add an effective transverse field by pulsed application of a microwave drive. At a critical interaction-to-drive ratio, we observe a bifurcation in the mean-field dynamics which is associated with a ground-state phase transition from paramagnetic to ferromagnetic. By optically imprinting a spatially varying interaction strength,

we directly observe this bifurcation as a function of position in the atomic cloud.

The principle of our experiments is illustrated in Fig. 1. To generate Ising interactions for spins encoded in two hyperfine ground states $|\downarrow\rangle = |6S_{1/2}, F = 3, m_F = 0\rangle$ and $|\uparrow\rangle = |6S_{1/2}, F = 4, m_F = 0\rangle$, we couple state $|\uparrow\rangle$ to the Rydberg manifold $|R\rangle = |43P_{3/2}\rangle$ with a 319 nm laser field of Rabi frequency Ω and detuning Δ from the $|43P_{3/2}, m_J = 3/2\rangle$ state. For large detuning $\Delta > \Omega$, the dominant effect of the dressing light on a single atom in state $|\uparrow\rangle$ is an ac Stark shift given by $\Omega^2/(4\Delta)$. However, for two atoms separated by a distance r, the ac Stark shift is modified by Rydberg interactions $V_R(r)$, which suppress a virtual process in which both atoms are simultaneously excited [Fig. 1(b)]. The result is an effective interaction $J(r)$ between atoms in state $|\uparrow\rangle$.

The ground-state dynamics are then described by an interaction Hamiltonian

$$H = \sum_{i>j} J(\mathbf{r}_i - \mathbf{r}_j)\left(s_i^z + 1/2\right)\left(s_j^z + 1/2\right). \qquad (1)$$

This Hamiltonian includes the desired Ising interactions,

$$H_{ZZ} = \sum_{i>j} J(r_{ij}) s_i^z s_j^z, \qquad (2)$$

and a density-dependent effective field (terms $\propto s_i^z$ in Eq. 1) that can be removed by spin echo. The characteristic strength of the interactions is given by $|J_0| = \Omega^4/|8\Delta^3|$ (where we set $\hbar = 1$), and the sign is determined by Δ, with $\Delta > 0$ producing ferromagnetic interactions ($J_0 < 0$). The characteristic range r_c is set by the condition $V_R(r_c, \theta) = \Delta$ and is angle-dependent when dressing with P states [55].

To achieve a large interaction range while remaining in the dressing regime $\Delta \gg \Omega$, it is advantageous to have a strong Rydberg-Rydberg interaction. To this end, we operate in the vicinity of a Förster resonance, i.e., a near degeneracy between the energies of the $|nP_{3/2}; nP_{3/2}\rangle$ and $|nS_{1/2}; (n+1)S_{1/2}\rangle$ pair states that enhances the interaction strength [56]. We select $n = 43$, which yields a small Förster defect $\Delta_F = 2\pi \times 42$ MHz [57] and hence strong interactions even at zero electric field. We couple to state $|R\rangle$ with σ^+-polarized light, resulting in an interaction range $r_c \lesssim 5$ μm for our typical detuning. We apply this light to a gas of cesium atoms at a temperature $T = 23$ μK and typical density $\rho \sim 10^{11}$ cm^{-3}, confined in an optical dipole trap with a 50 μm waist.

We observe the Rydberg-dressed interactions by Ramsey spectroscopy. In particular, the Ising interactions in Eq. 1 cause each spin to precess at a rate that depends on the number of surrounding atoms in state $|\uparrow\rangle$. For a system of spins each initialized in state $|\theta\rangle = \sin(\theta/2)|\downarrow\rangle + \cos(\theta/2)|\uparrow\rangle$, we thus expect the average precession rate to depend on the tilt θ. We measure this effect using a spin echo sequence, shown in Fig. 2(a),

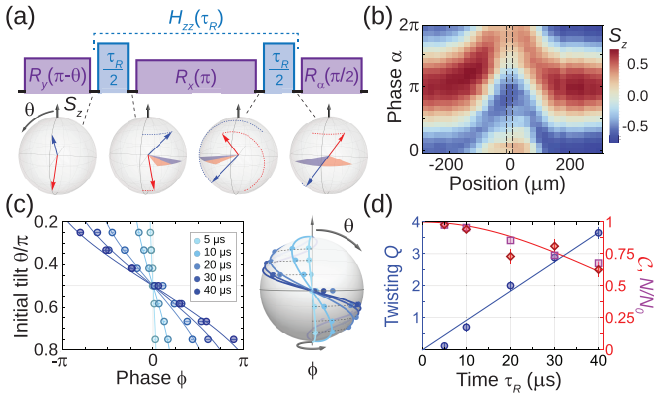

FIG. 2. **Measuring Ising interactions.** (a) Ramsey sequence with spin echo. Bloch spheres show average spin $\langle \mathbf{S} \rangle$ at select times for two different initial states $|\theta\rangle$ (blue and red). (b) Interference fringe for $|\theta\rangle = |3\pi/4\rangle$ showing spatial dependence of interaction-induced phase shift. Black dashed lines show analysis region for subplots (c-d). (c) Phase shift ϕ vs. initial tilt θ for different interaction times τ_R with fit curves $\phi = Q\cos\theta$. (d) Twisting strength Q (blue circles) vs. time, extracted from fits in (c). The slope of the linear fit (solid blue) gives the mean-field interaction energy $\chi = 2\pi \times 15(1)$ kHz. Also shown are interference contrast $\mathcal{C}$ (red diamonds with fit curve) and atom number N (magenta squares) remaining after Rydberg dressing, normalized to initial atom number N_0.

which removes the s^z-independent ac Stark shift due to the dressing light and leaves behind only the phase shift resulting from Ising interactions. We extract this phase shift by fitting an interference fringe obtained by varying the phase α of the final $\pi/2$ pulse and detecting the resulting populations in states $|\uparrow\rangle$ and $|\downarrow\rangle$ by fluorescence imaging.

Figure 2(b) shows a typical Ramsey fringe for determining the mean-field shift in an initial state $|\theta = 3\pi/4\rangle$. We illuminate only a 160 μm wide region of an elongated atomic cloud with the dressing light, and thus directly observe the spatial variation of the interaction strength due to the approximately Gaussian beam profile. The measurement is performed with a peak Rabi frequency $\Omega = 2\pi \times 1.9(3)$ MHz, determined from the total ac Stark shift in Ramsey measurements at large detuning without spin echo. We operate at a detuning $\Delta = 2\pi \times 21.0(3)$ MHz that empirically optimizes the ratio of coherent interactions to loss [55]. Dressing for a total time $\tau_R = 40$ μs yields a peak interaction-induced phase shift $\phi = 2.6$ rad.

To more fully characterize the interactions, we perform Ramsey measurements with different initial states $|\theta\rangle$ and interaction times τ_R. We analyze the central region of the cloud, shown by the dashed lines in Fig. 2(b). The final phase ϕ of the average Bloch vector $|\theta, \phi\rangle = \sin(\theta/2)|\downarrow\rangle + e^{i\phi}\cos(\theta/2)|\uparrow\rangle$ is shown in Fig. 2(c) with different shades representing dressing times ranging from

5 μs to 40 μs. We observe characteristic one-axis twisting dynamics, where the $\phi = 0$ meridian of the Bloch sphere, on which all states are initially prepared, becomes twisted about the z-axis due to the $\langle s^z \rangle$-dependent spin precession rate.

Fitting the twisting by $\phi = Q\cos(\theta)$ yields a linear dependence of twisting strength Q on interaction time τ_R. The slope $\chi \equiv |dQ/d\tau_R|$ indicates the mean-field interaction strength. The measured mean-field shift is approximately 3.5 times larger than the prediction $\chi_{\rm th} = (\rho/2)\int J(\mathbf{r})\mathrm{d}^3\mathbf{r}$ based on the calculated interaction potential and density $\rho = 1.4 \times 10^{11}$ cm^{-3} [55]. We attribute this to weak incoherent excitation of the $|43P_{3/2}\rangle$ state, which can effectively increase the interaction strength, albeit in a dissipative manner. This dissipative effect dominates for $\tau_R > 1/\gamma_L$, where γ_L is the laser linewidth, and may be slightly exacerbated by blackbody decay to other Rydberg states [55]. It can be largely echoed away in a sequence of short Rydberg pulses with more frequent π pulses, which we present further below. There, the measured interaction strength is consistent with the dressed potentials and atomic density.

The dynamics we observe are similar to those of the one-axis twisting Hamiltonian $H = -\chi S_z^2/N$, where $\mathbf{S} = \sum_{i=1}^{N} \mathbf{s}_i$ represents the collective spin of $N = 2S$ atoms. This description would be exact if the interactions had infinite range, a case well-studied as a mechanism for spin squeezing [52]. For finite-range Ising interactions, we reach a particular twisting rate via stronger pairwise interactions among fewer atoms than would be required if each atom interacted with all others. One expected consequence is a shortening of the collective Bloch vector, corresponding to a reduction in contrast $\mathcal{C} = |\langle \mathbf{S} \rangle|/S$ [53, 58]. In Fig. 2(d), we attribute the contrast decay to a combination of finite interaction range and inhomogenous broadening associated with incoherent Rydberg excitation. The contrast maintained places a lower bound $N_c \gtrsim 14$ on the number of atoms within a typical interaction sphere [55], which corroborates the applicability of the mean-field model.

To realize the full transverse-field Ising model, we additionally apply a microwave coupling between the two ground states $|\uparrow\rangle$ and $|\downarrow\rangle$. Since we require a spin echo sequence to obtain Ising interactions H_{ZZ} with no additional ac Stark shifts, it is convenient to emulate the transverse-field Ising model by rapidly alternating between applying interactions H_{ZZ} for a time τ_R and the transverse field $H_X = \sum_i h s_i^x$ for a time τ_X. One application each of H_{ZZ} and H_X defines our Floquet cycle. When both the interaction and the rotation per Floquet cycle are small — i.e., when $\chi\tau_R \ll 1$ and $h\tau_X \ll 1$ — the effective Hamiltonian becomes equivalent to a static transverse-field Ising model:

$$H_{\rm eff} \propto \tau_R H_{ZZ} + \tau_X H_X. \qquad (3)$$

For ferromagnetic interactions, the Hamiltonian $H_{\rm eff}$ theoretically undergoes a phase transition as a function of the ratio $\Lambda \equiv \chi\tau_R/(h\tau_X)$ of interaction strength to transverse field. When the transverse field dominates ($\Lambda \ll 1$), the ground state is paramagnetic, with all spins aligned along the x-axis. In the limit where Ising interactions dominate ($\Lambda \gg 1$), there are two degenerate ground states with all spins aligned along $\pm\hat{\mathbf{z}}$. Even without directly preparing these ground states, we can look for signatures of the paramagnetic-ferromagnetic phase transition in the mean-field dynamics.

We probe the dynamics of the transverse-field Ising model by varying the number of Floquet cycles to measure trajectories on the Bloch sphere for different initial states [Fig. 3(a)]. After initializing in a state $|\theta, \phi\rangle$, we alternately apply Ising interactions and microwave rotations for $(\tau_R, \tau_X) = (10, 1)$ μs. After applying up to $k = 4$ Floquet cycles as shown in Fig. 3(b), we either directly measure S_z by state-sensitive imaging or measure

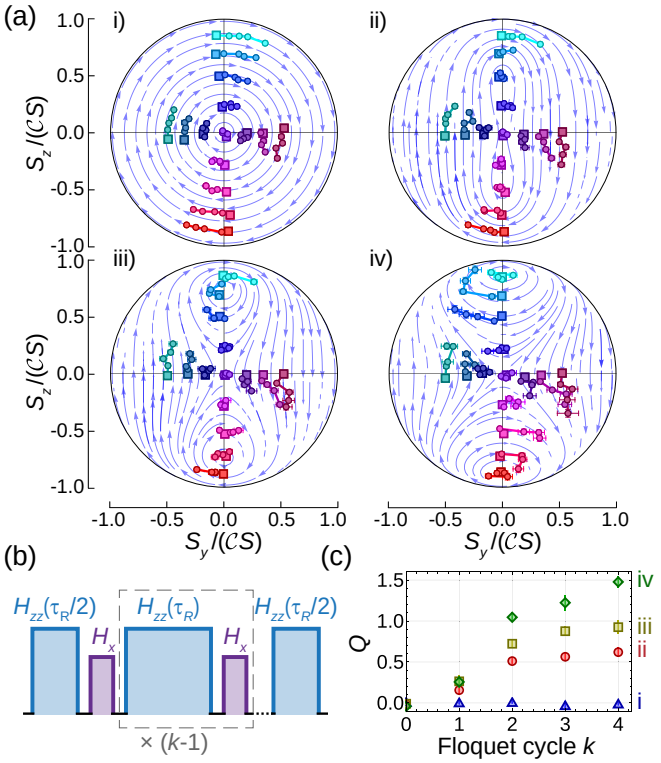

FIG. 3. **Transverse-field Ising dynamics.** (a) Trajectories $\mathbf{S}(k)$ for initial states $|\theta, \phi\rangle$ (square data points) and up to $k = 4$ Floquet cycles, obtained with dressing parameters $(\Omega, \Delta) = 2\pi \times (2.8, 25)$ MHz. Plots (i-iv) are for $\Lambda_{\rm eff} = 0, 1.2(2), 1.8(3), 2.7(4)$. Blue flow lines show mean-field theory for best fit $\Lambda = 0, 1.1, 1.5, 2.2$. (b) Sequence of microwave (purple) and Rydberg dressing (blue) pulses for k Floquet cycles. The first application of H_{ZZ} is split into two, with the second Rydberg pulse after the last microwave rotation, to keep the fixed points along the $\phi = 0$ meridian. (c) Twisting strength Q vs. k measured with $(\tau_R, \tau_X) = (10, 0)$ μs in the four regions of the atomic cloud (i-iv) used in part (a).

(S_x, S_y) by first applying a $\pi/2$ microwave pulse of variable phase. We then plot the trajectory of the normalized Bloch vector $\mathbf{S}/(\mathcal{C}S)$. Due to the spatial variation of the interaction strength χ, a single such data set allows us to observe the dependence of the trajectory on χ at fixed rotation angle $h\tau_X = 0.12(1)$. Figs. 3(a.i-iv) show trajectories at four representative interaction strengths.

We compare the observed trajectories with a mean-field model, in which the system is described by a classical Hamiltonian $H_{\mathrm{MF}} \propto -\Lambda S_z^2/N - S_x$. The ground states of H_{MF} are fixed points of the collective spin dynamics, and can readily be calculated for a given interaction-to-drive ratio Λ. For $\Lambda < 1$, there is only a single fixed point at $\mathbf{S} = S\hat{\mathbf{x}}$ (the paramagnetic ground state). Above a critical ratio $\Lambda = 1$, this fixed point bifurcates into two stable fixed points (ferromagnetic ground states) at positions

$$\mathbf{S}/S = (1/\Lambda, 0, \pm\sqrt{1 - 1/\Lambda^2}), \tag{4}$$

while one unstable fixed point remains on the x-axis. Flow lines derived from this mean-field model are shown in Fig. 3(a) (blue curves).

The mean-field model qualitatively explains the dynamics we observe. Whereas the Bloch vectors precess about $\hat{\mathbf{x}}$ for weak interactions, above a critical interaction strength they instead begin to precess about two new fixed points in the xz-plane. For a quantitative comparison, we must account for effects of dissipation and interaction-induced dephasing. First, we observe a decrease in interaction strength χ for later Floquet cycles [Fig. 3(c)], which we attribute to loss and decay of Rydberg atoms. The given values of χ are the averages over the four Floquet cycles. Second, we observe a reduction in contrast $\mathcal{C}$, whose effect on the fixed-point positions is described by replacing Λ in Eq. 4 by $\Lambda_{\mathrm{eff}} \equiv \mathcal{C}\Lambda$ [55]. Independently measured values of Λ_{eff} are within 20% of values obtained by fitting the mean-field model to the trajectories.

The spatially varying interaction strength allows us to directly observe the bifurcation of the fixed points as a function of position in the atomic cloud. In Fig. 4(a), we observe the spatial dependence of the phase ϕ after four Floquet cycles for different initial states $|\theta\rangle$. Fixed points are revealed by the white contour level, where $\phi = 0$. Outside of the dressing beam (e.g., at position A), a single fixed point is visible at $\theta = \pi/2$, corresponding to the paramagnetic ground state. At a critical interaction strength, the stable fixed point bifurcates and all three fixed points become visible. We interpret this bifurcation as a signature of the paramagnetic-ferromagnetic phase transition, which theoretically occurs at $\mathcal{C}\chi\tau_R = h\tau_X$.

To compare the position of the critical point with theory, we calibrate the spatial dependence of the interaction strength by an analogous measurement with no transverse field [Fig. 4(b)]. We plot and fit the spatial dependence of $\mathcal{C}\chi\tau_R$ in Fig. 4(c), accounting for the spatially

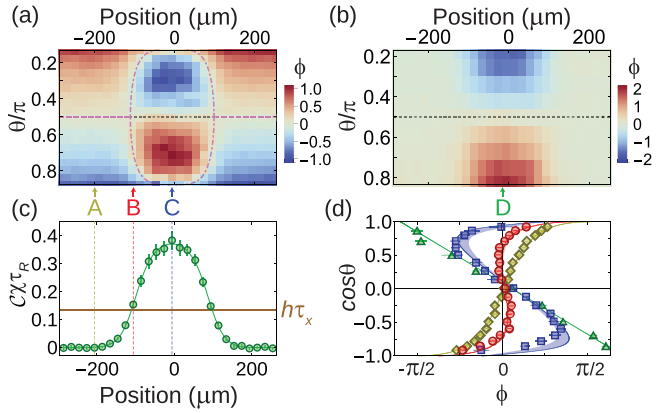

FIG. 4. **Bifurcation of fixed points,** signifying paramagnetic and ferromagnetic ground states. We measure the phase ϕ after $k = 4$ Floquet cycles with (a) $h\tau_X = 0.14(1)$ or (b) $h\tau_X = 0$, as a function of initial tilt θ and position. The $\phi = 0$ contour reveals fixed points of the mean-field dynamics, matching the theoretical prediction (purple dot-dashed, purple dashed, and gray dotted curves for the ferromagnetic ground states, paramagnetic ground state, and unstable fixed points, respectively). Fitting the phase evolution in (b) yields the average mean-field interaction $\chi\tau_R$ per cycle. (c) Green points and fit curve show $\mathcal{C}\chi\tau_R$ vs. position, compared with rotation angle $h\tau_x$ (brown line). (d) Final phase ϕ vs. initial tilt θ for cuts labeled A (yellow diamonds), B (red circles), C (blue squares), and D (green triangles), in order of increasing $|\Lambda|$. Solid lines show Floquet mean-field model for the measured values $\chi\tau_R$ and $h\tau_X$ with no contrast loss, while edge of shaded region accounts for contrast $\mathcal{C}$.

varying contrast $\mathcal{C} \gtrsim 0.7$. Comparing with the value $h\tau_X = 0.14(1)$ yields a prediction for the positions of the fixed points shown by the purple curve in Fig. 4(a). In Fig. 4(d), we furthermore compare the full dependence of final phase ϕ on initial tilt θ with a mean-field model of the Floquet sequence. This model is shown by the solid curves, which incorporate the independently measured values $\chi\tau_R$ and $h\tau_X$ and include only a small phase offset as a free parameter. The full phase evolution, including the fixed-point positions, is well described by the mean-field model.

The dynamical timescales accessible in our current experiments are limited by atom loss and by motion into and out of the dressing region. These effects can be reduced in future experiments by reducing the laser linewidth and trapping the atoms in a lattice or tweezer array [3]. Future work may also explore the use of electric fields, molecular bound states [15, 59], microwave dressing [60] and/or adiabatic protocols [61] to achieve interaction-to-decay ratios approaching the ratio $\Omega/\Gamma \gtrsim 10^3$ of Rabi frequency to Rydberg state linewidth [55].

Our work opens prospects in quantum simulation benefiting from spatiotemporal control of interactions, including exploring quantum criticality in both driven [29] and spatially inhomogeneous [31] systems. Whereas here

we have emulated a static transverse-field Ising model, varying the strength of interaction and/or rotation per Floquet cycle will allow for accessing quantum phases with no equilibrium analog [28, 62], including Floquet symmetry-protected topological phases [16, 28]. Combining Floquet driving with a spatially varying interaction strength may allow for realizing quantum systems with emergent spacetime curvature [63, 64]. The Ising interactions demonstrated here can furthermore be applied to generate entangled states for enhanced clocks or sensors [34, 53], with dynamical control of interactions and the transverse field enabling enhanced spin squeezing [36]. Spatial addressing will additionally allow for preparing arrays of entangled states for optimal atomic clocks [65, 66].

This work was supported by the ARO and the ONR. V. Borish acknowledges support from the NSF GRFP and the DARE Doctoral Fellowship. O. Marković acknowledges support from the Serbian Foundation for Talented Youth. J. Hines acknowledges support from the NDSEG Fellowship. J. Hines and M. Schleier-Smith acknowledge support from the DOE Office of Science, Office of Basic Energy Sciences, under grant number DE-SC0019174. We acknowledge technical assistance from Michelle Chong and Josie Meyer and discussions with Leo Hollberg.

[1] P. Schauß, M. Cheneau, M. Endres, T. Fukuhara, S. Hild, A. Omran, T. Pohl, C. Gross, S. Kuhr, and I. Bloch, Nature **491**, 87 (2012).
[2] J. Zeiher, R. Van Bijnen, P. Schauß, S. Hild, J.-y. Choi, T. Pohl, I. Bloch, and C. Gross, Nat. Phys. **12**, 1095 (2016).
[3] J. Zeiher, J.-Y. Choi, A. Rubio-Abadal, T. Pohl, R. van Bijnen, I. Bloch, and C. Gross, Phys. Rev. X **7**, 041063 (2017).
[4] H. Labuhn, D. Barredo, S. Ravets, S. De Léséleuc, T. Macrì, T. Lahaye, and A. Browaeys, Nature **534**, 667 (2016).
[5] H. Bernien, S. Schwartz, A. Keesling, H. Levine, A. Omran, H. Pichler, S. Choi, A. S. Zibrov, M. Endres, M. Greiner, et al., Nature **551**, 579 (2017).
[6] S. de Léséleuc, V. Lienhard, P. Scholl, D. Barredo, S. Weber, N. Lang, H. P. Büchler, T. Lahaye, and A. Browaeys, Science **365**, 775 (2019).
[7] A. P. Orioli, A. Signoles, H. Wildhagen, G. Günter, J. Berges, S. Whitlock, and M. Weidemüller, Phys. Rev. Lett. **120**, 063601 (2018).
[8] E. Guardado-Sanchez, P. T. Brown, D. Mitra, T. Devakul, D. A. Huse, P. Schauß, and W. S. Bakr, Phys. Rev. X **8**, 021069 (2018).
[9] V. Lienhard, S. de Léséleuc, D. Barredo, T. Lahaye, A. Browaeys, M. Schuler, L.-P. Henry, and A. M. Läuchli, Phys. Rev. X **8**, 021070 (2018).
[10] M. Landini, N. Dogra, K. Kröger, L. Hruby, T. Donner, and T. Esslinger, Phys. Rev. Lett. **120**, 223602 (2018).
[11] Y. Guo, R. M. Kroeze, V. D. Vaidya, J. Keeling, and B. L. Lev, Phys. Rev. Lett. **122**, 193601 (2019).
[12] E. J. Davis, G. Bentsen, L. Homeier, T. Li, and M. H. Schleier-Smith, Phys. Rev. Lett. **122**, 010405 (2019).
[13] M. Yan, B. J. DeSalvo, B. Ramachandhran, H. Pu, and T. C. Killian, Phys. Rev. Lett. **110**, 123201 (2013).
[14] O. Thomas, C. Lippe, T. Eichert, and H. Ott, Nat. Commun. **9**, 2238 (2018).
[15] R. M. W. van Bijnen and T. Pohl, Phys. Rev. Lett. **114**, 243002 (2015).
[16] I.-D. Potirniche, A. C. Potter, M. Schleier-Smith, A. Vishwanath, and N. Y. Yao, Phys. Rev. Lett. **119**, 123601 (2017).
[17] G. Pupillo, A. Micheli, M. Boninsegni, I. Lesanovsky, and P. Zoller, Phys. Rev. Lett. **104**, 223002 (2010).
[18] J. E. Johnson and S. L. Rolston, Phys. Rev. A **82**, 033412 (2010).
[19] N. Henkel, R. Nath, and T. Pohl, Phys. Rev. Lett. **104**, 195302 (2010).
[20] E. Urban, T. A. Johnson, T. Henage, L. Isenhower, D. D. Yavuz, T. G. Walker, and M. Saffman, Nat. Phys. **5**, 110 (2009).
[21] A. Gaëtan, Y. Miroshnychenko, T. Wilk, A. Chotia, M. Viteau, D. Comparat, P. Pillet, A. Browaeys, and P. Grangier, Nat. Phys. **5**, 115 (2009).
[22] X. L. Zhang, L. Isenhower, A. T. Gill, T. G. Walker, and M. Saffman, Phys. Rev. A **82**, 030306(R) (2010).
[23] T. Wilk, A. Gaëtan, C. Evellin, J. Wolters, Y. Miroshnychenko, P. Grangier, and A. Browaeys, Phys. Rev. Lett. **104**, 010502 (2010).
[24] Y.-Y. Jau, A. M. Hankin, T. Keating, I. H. Deutsch, and G. W. Biedermann, Nat. Phys. **12**, 71 (2016).
[25] I. D. Leroux, M. H. Schleier-Smith, and V. Vuletić, Phys. Rev. Lett. **104**, 073602 (2010).
[26] O. Hosten, R. Krishnakumar, N. J. Engelsen, and M. A. Kasevich, Science **352**, 1552 (2016).
[27] I. Bouchoule and K. Mølmer, Phys. Rev. A **65**, 041803(R) (2002).
[28] V. Khemani, A. Lazarides, R. Moessner, and S. L. Sondhi, Phys. Rev. Lett. **116**, 250401 (2016).
[29] W. Berdanier, M. Kolodrubetz, S. Parameswaran, and R. Vasseur, Proc. Natl. Acad. Sci. U.S.A. **115**, 9491 (2018).
[30] A. Lerose, J. Marino, A. Gambassi, and A. Silva, Phys. Rev. B **100**, 104306 (2019).
[31] F. J. Gómez-Ruiz and A. del Campo, Phys. Rev. Lett. **122**, 080604 (2019).
[32] A. W. Glaetzle, R. M. van Bijnen, P. Zoller, and W. Lechner, Nat. Commun. **8**, 15813 (2017).
[33] H. Pichler, S.-T. Wang, L. Zhou, S. Choi, and M. D. Lukin, arXiv:1808.10816 [quant-ph] (2018).
[34] E. Davis, G. Bentsen, and M. Schleier-Smith, Phys. Rev. Lett. **116**, 053601 (2016).
[35] T. Macrì, A. Smerzi, and L. Pezzè, Phys. Rev. A **94**, 010102(R) (2016).
[36] R. Kaubruegger, P. Silvi, C. Kokail, R. van Bijnen, A. M. Rey, J. Ye, A. M. Kaufman, and P. Zoller, arXiv:1908.08343 [quant-ph] (2019).
[37] F. K. Fatemi, K. M. Jones, and P. D. Lett, Phys. Rev. Lett. **85**, 4462 (2000).
[38] G. Thalhammer, M. Theis, K. Winkler, R. Grimm, and J. H. Denschlag, Phys. Rev. A **71**, 033403 (2005).
[39] K. Enomoto, K. Kasa, M. Kitagawa, and Y. Takahashi, Phys. Rev. Lett. **101**, 203201 (2008).
[40] S. Blatt, T. L. Nicholson, B. J. Bloom, J. R. Williams,

J. W. Thomsen, P. S. Julienne, and J. Ye, Phys. Rev. Lett. **107**, 073202 (2011).
[41] L. W. Clark, L.-C. Ha, C.-Y. Xu, and C. Chin, Phys. Rev. Lett. **115**, 155301 (2015).
[42] J. B. Balewski, A. T. Krupp, A. Gaj, S. Hofferberth, R. Löw, and T. Pfau, New J. Phys. **16**, 063012 (2014).
[43] C. Gaul, B. J. DeSalvo, J. A. Aman, F. B. Dunning, T. C. Killian, and T. Pohl, Phys. Rev. Lett. **116**, 243001 (2016).
[44] E. A. Goldschmidt, T. Boulier, R. C. Brown, S. B. Koller, J. T. Young, A. V. Gorshkov, S. L. Rolston, and J. V. Porto, Phys. Rev. Lett. **116**, 113001 (2016).
[45] T. Boulier, E. Magnan, C. Bracamontes, J. Maslek, E. A. Goldschmidt, J. T. Young, A. V. Gorshkov, S. L. Rolston, and J. V. Porto, Phys. Rev. A **96**, 053409 (2017).
[46] J. A. Aman, B. J. DeSalvo, F. B. Dunning, T. C. Killian, S. Yoshida, and J. Burgdörfer, Phys. Rev. A **93**, 043425 (2016).
[47] A. Arias, G. Lochead, T. M. Wintermantel, S. Helmrich, and S. Whitlock, Phys. Rev. Lett. **122**, 053601 (2019).
[48] T. Zibold, E. Nicklas, C. Gross, and M. K. Oberthaler, Phys. Rev. Lett. **105**, 204101 (2010).
[49] A. Friedenauer, H. Schmitz, J. T. Glueckert, D. Porras, and T. Schätz, Nat. Phys. **4**, 757 (2008).
[50] R. Islam, E. E. Edwards, K. Kim, S. Korenblit, C. Noh, H. Carmichael, G.-D. Lin, L.-M. Duan, C.-C. J. Wang, J. K. Freericks, et al., Nat. Commun. **2**, 377 (2011).
[51] J. Zhang, P. Hess, A. Kyprianidis, P. Becker, A. Lee, J. Smith, G. Pagano, I.-D. Potirniche, A. C. Potter, A. Vishwanath, et al., Nature **543**, 217 (2017).
[52] M. Kitagawa and M. Ueda, Phys. Rev. A **47**, 5138 (1993).
[53] L. I. R. Gil, R. Mukherjee, E. M. Bridge, M. P. A. Jones, and T. Pohl, Phys. Rev. Lett. **112**, 103601 (2014).
[54] R. Mukherjee, T. C. Killian, and K. R. A. Hazzard, Phys. Rev. A **94**, 053422 (2016).
[55] See Supplemental Material at [URL will be inserted by publisher] for supporting derivations and additional experimental details, which includes Ref. [67].
[56] T. Vogt, M. Viteau, J. Zhao, A. Chotia, D. Comparat, and P. Pillet, Phys. Rev. Lett. **97**, 083003 (2006).
[57] N. Šibalić, J. D. Pritchard, K. J. Weatherill, and C. S. Adams, Comput. Phys. Commun. **220**, 319 (2017).
[58] M. Foss-Feig, K. R. A. Hazzard, J. J. Bollinger, and A. M. Rey, Phys. Rev. A **87**, 042101 (2013).
[59] S. Hollerith, J. Zeiher, J. Rui, A. Rubio-Abadal, V. Walther, T. Pohl, D. M. Stamper-Kurn, I. Bloch, and C. Gross, Science **364**, 664 (2019).
[60] D. Petrosyan and K. Mølmer, Phys. Rev. Lett. **113**, 123003 (2014).
[61] T. Keating, R. L. Cook, A. M. Hankin, Y.-Y. Jau, G. W. Biedermann, and I. H. Deutsch, Phys. Rev. A **91**, 012337 (2015).
[62] D. V. Else, B. Bauer, and C. Nayak, Phys. Rev. Lett. **117**, 090402 (2016).
[63] B. Lapierre, K. Choo, C. Tauber, A. Tiwari, T. Neupert, and R. Chitra, arXiv:1909.08618 [cond-mat.str-el] (2019).
[64] R. Fan, Y. Gu, A. Vishwanath, and X. Wen, arXiv:1908.05289 [cond-mat.str-el] (2019).
[65] E. M. Kessler, P. Komar, M. Bishof, L. Jiang, A. S. Sørensen, J. Ye, and M. D. Lukin, Phys. Rev. Lett. **112**, 190403 (2014).
[66] V. Bužek, R. Derka, and S. Massar, Phys. Rev. Lett. **82**, 2207 (1999).
[67] J. Léonard, M. Lee, A. Morales, T. M. Karg, T. Esslinger, and T. Donner, New J. Phys. **16**, 093028 (2014).